Review Article

Rates and Mechanisms of Electron Transfer/Nickel-Catalyzed Homocoupling and Carboxylation Reactions. An Electrochemical Approach†

Christian Amatore* and Anny Jutand

Ecole Normale Supérieure, Laboratoire de Chimie, URA CNRS 1110, 24 rue Lhomond, F-752 31 Paris CEDEX 05, France

Amatore, C. and Jutand, A., 1990. Rates and Mechanisms of Electron Transfer/Nickel-Catalyzed Homocoupling and Carboxylation Reactions. An Electrochemical Approach. – Acta Chem. Scand. 44: 755–764.

The conceptual analogies existing between electrochemically initiated homogeneous reactions and their equivalent taking place at the surface of metal particles are presented. With these analogies in mind we propose an electrochemical approach to the investigation of the rates and mechanisms of homocoupling and carboxylation of aryl halides catalyzed by nickel complexes where reduction is the driving force. It is thus shown that nickel catalysis of the homocoupling reaction occurs via an efficient sequence involving both paramagnetic (Ni^{I} and Ni^{III}) and diamagnetic (Ni^{0} and Ni^{II}) organometallic nickel complexes. In the presence of carbon dioxide, this chain is annihilated and a new chain develops which affords high carboxylation yields. The transposition of these results to 'homogeneous' conditions, involving metal particles instead of a cathode, is discussed and its validity is examined on the basis of previously reported kinetic results.

Since the original work of Semmelhack and his group,[1] classical procedures for the synthesis of symmetrical or unsymmetrical biaryls from aryl halides have been supplanted by those involving zero-valent transition metals. These methods which were initially based on stoichiometric quantities of a zero-valent transition metal were later shown by several authors to require, in fact, only catalytic amounts of the zero-valent metal, provided that stoichiometric[2] or excess[3] quantities of a reducing agent are used. For most reported synthetic procedures the reducing agent consists of particles of a reducing metal such as Zn, Mg, Mn, etc., however, it has also been shown that the reducing driving force could be provided by electrochemical means.[4,5]

Several attempts to delineate the role of the zero-valent transition metal catalyst have been made.[3,6] Yet because of the difficulty of measuring kinetics at the surface of a metal powder particle, most of the quantitative mechanistic work in the area corresponds to homogeneous situations, i.e. to stoichiometric conditions for the zero-valent transition metal.[6] There is general agreement that the catalytic cycle is initiated by oxidative addition of the aromatic halide to the zero-valent metal to afford an arylmetal(II) intermediate[7] [eqn. (1)] and is terminated by the reductive elimination of a diarylmetal(III) species[3,6,8] into a biaryl and a metal(I) moiety which is reduced to its zero-valent active form [eqns. (2) and (3)].

$$ArX + M^{0} \longrightarrow Ar-M^{II}-X \quad (1)$$

$$(Ar)_2M^{III}X \longrightarrow Ar\text{–}Ar + M^{I}X \quad (2)$$

$$M^{I}X + \text{Reductant} \longrightarrow M^{0}, \text{ etc.} \quad (3)$$

Tsou and Kochi[6] proposed a radical chain mechanism, involving intermediate paramagnetic nickel complexes, to explain the formation of the diarylnickel(III) species, under conditions stoichiometric in zero-valent nickel. However the exact mechanistic sequence leading to the diarylnickel(III) from the initial arylnickel(II), was not clear for catalytic conditions, i.e. in the presence of a reducing metal. Colon and Kelsey[9] proposed a tentative mechanism for such conditions, yet they concluded that 'although a full mechanistic understanding of this complex reaction awaits further study, we believe the mechanism [we] proposed [...] accommodates our experimental data better than any mechanism previously proposed. Further research may provide refinements of this mechanistic model, but we suspect that the crucial role of the metal in the reduction of an arylnickel species will remain a central feature of the coupling of aryl chlorides.'

† This contribution is based on a main section lecture by C. Amatore at the 32nd IUPAC Congress (Section VI: Electron Transfer Reactions) in Stockholm, Sweden, August 2–7, 1989.

* To whom correspondence should be addressed.

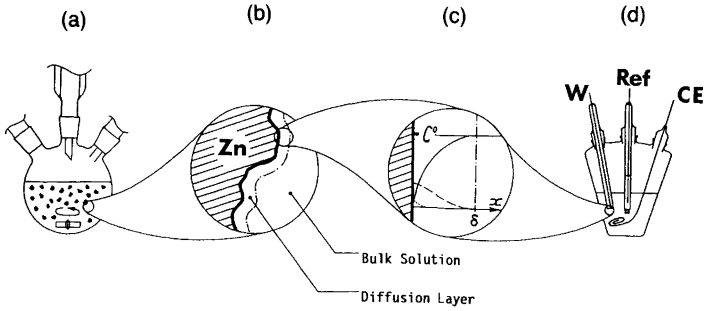

Fig. 1. Schematic representation of the microstructure of solutions at a metal particle or an electrode surface: (a) 'homogeneous' reaction vessel; (b) representation of the diffusion layer (a few tens of micrometers) and of the bulk solution, at a metal particle/solution interface; (c) concentration profiles developing within the diffusion layer ($x \leq \delta$) existing at the surface of a zinc metal particle or of an electrode, in the case of the pyrylium cation reduction discussed in the text. $C°$: initial pyrylium concentration; (———) pyrylium cation concentration; (·····) pyrylium radical concentration; (-----) 4,4′-dimer concentration; (d) electrochemical cell. W, working electrode; Ref, reference electrode; CE, counter electrode.

Indeed, a detailed kinetic investigation of reactions taking place near the surface of metal particles distributed 'homogeneously' in a solution is extremely difficult or even impossible. As illustrated in Figs. 1(b)–(c), the solution near a metal particle surface can be separated schematically into two regions.[10] Outside a layer of solution adjacent to the metal surface, the thickness of which (a few tens of micrometers) depends on the exact hydrodynamics of the solution, the solution – termed the bulk solution – is microscopically homogeneous as a result of convection. Inside the layer adjacent to the electrode – termed the diffusion layer – no convection occurs and the reactant(s) and product(s) diffuse to or from the metal surface while they undergo chemical reaction(s). When the reaction(s) initiated at the metal surface are sufficiently fast, i.e. involve intermediates of lifetimes smaller than ca. 100 ms under usual experimental conditions, none of these latter can escape the diffusion layer. Therefore kinetic analysis of the bulk solution composition as a function of time reflects only the overall result of the reaction(s) taking place in the solution and does not permit the identification of any intermediates. To illustrate this point, let us consider one of the most simple kinetic sequences that may take place at a particle surface. For example, reduction of pyrylium cations by zinc powder affords quantitatively the corresponding 4,4′-dimer according to eqn. (4). When the 4-position is substituted this dimer is the final product, whereas it reacts further to yield a bipyranylidene in the opposite case.[11] For the sake of simplification in this presentation we will restrict the following discussion to the case of 4-substituted pyrylium cations.

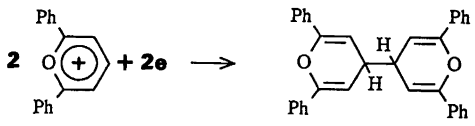

(4)

Assuming that the size distribution of the zinc particles is even, the kinetics of disappearance of the pyrylium cation (denoted Py^+), or of appearance of the dimer (denoted Py–Py), in the bulk solution correspond to an apparent rate law first order in pyrylium and first order in zinc surface area. For zinc particles of a given uniform size, a zinc 'concentration' may be defined as the number of moles of zinc divided by the volume of the solution, which leads to the following rate law given in eqn. (5) where k^{app} is an

$$v = -\mathrm{d}[Py^+]/\mathrm{d}t = \tfrac{1}{2}\,\mathrm{d}[Py\text{–}Py]/\mathrm{d}t = k^{app}[Py^+][Zn] \qquad (5)$$

apparent rate constant which depends on the particle shape and on the hydrodynamics of the solution. It is seen that such a rate law imparts almost no kinetic information on the very mechanism of the dimer formation, because it reflects only modifications of the bulk solution, whereas the coupling step occurs within the diffusion layer, that is within few tens of Ångströms from the zinc particle surface. On the other hand, investigation of the same reaction by electrochemistry in the nanosecond timescale,[12] i.e. when the zinc reductant is replaced by a ultramicroelectrode of comparable size (10 μm diameter disk electrode), revealed that the mechanism for the dimer formation is given by eqns. (6) and (7), and that, for 2,6-diphenylpyrylium, the

$$Py^+ + e \rightleftharpoons Py^{\cdot} \qquad (6)$$

$$2\ Py^{\cdot} \longrightarrow Py\text{–}Py \qquad (7)$$

rate constant of the duplication step is close to the diffusion limit, i.e., $k = 2.5\times10^9\ M^{-1}\ s^{-1}$.[12]

One may wonder how electrochemistry may provide such information, which is not accessible by classical ways. This arises because electrochemistry probes the diffusion layer composition 'from the inside,' i.e. provides kinetic information relative to the composition of the very region of space where the reaction happens. Indeed, as shown on Fig. 1(c), the electrode solution interface is structured in a fashion similar to that described above for a particle/solution interface. However, now all kinetic data are sampled at the electrode surface and depend on the exact concentration profiles in the close vicinity (from ca. a few tens of Ångströms to several micrometers, depending on the timescale, e.g. on the scan rate considered in cyclic voltammetry)[13] of the electrode surface. Moreover the intermedi-

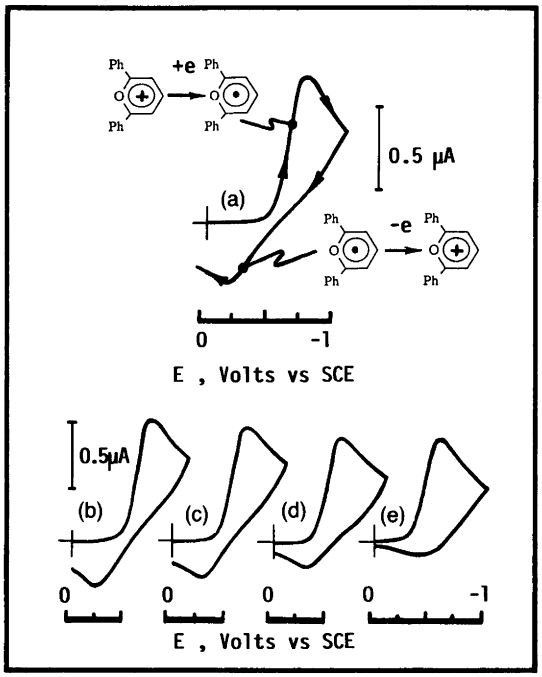

Fig. 2. Background-substracted cyclic voltammetry of 2,6-diphenylpyrylium perchlorate (10 mM) in acetonitrile, 0.1 M NBu_4BF_4 at 20 °C, at a platinum disk (Ø 10 μm) ultramicroelectrode as a function of scan rate v = 0.250 (a), 0.200 (b), 0.150 (c), 0.100 (d) and 0.075 (e) megavolts per second. The direction of potential scan variations are indicated by the arrows on the voltammogram in (a), together with each elementary electron transfer corresponding to the cathodic (top) and anodic (bottom) processes.

ates involved in the reaction scheme may often be 'seen' by their electrochemical signature. For example, in the above case [eqns. (6) and (7)], fast cyclic voltammetry in the megavolt per second range allowed the 'observation' of the pyrylium radical formed upon electron transfer, before it could dimerize. This intermediate, the life-time of which is ca. 20 ns under the experimental conditions exemplified by Fig. 2, is identified by its oxidation wave which develops when the scan rate is increased, i.e. when the time scale is made shorter and shorter [compare the anodic traces on the voltammograms (e) to (a) in Fig. 2].

The above simple example illustrates the great advantages of electrochemical techniques for the investigation of reactions which involve electron transfer steps taking place at a metal interface. On the one hand the reaction mechanism can be established on a sound basis. On the other hand, use of the recently available ultrafast cyclic voltammetry, with a timeresolution of a few tens of a nanosecond, allows identification of the key intermediates. In the following we show how these electrochemical approaches can be used with great profit in the investigation of the mechanism of aryl halides activation by catalytic zero-valent transition metals, in the presence of a reducing driving force. For this purpose we selected two examples taken from our research on the mechanism of activation of organic substrates by zero-valent transition metals.

Nickel Catalysis of Bromobenzene Homocoupling to Biphenyl.[14] In the above section we have shown the striking conceptual identities that exist in the different phenomena taking place at a metal particle or at an electrode surfaces. The experimental validity of these analogies is proved by the fact that when bromobenzene (9 mmol) is electrolyzed in the presence of 1 mmol $NiCl_2$(dppe) [dppe = 1,2-(diphenylphosphino)ethane], biphenyl is obtained quantitatively,[5] as it is under 'homogeneous' conditions[2,3] [eqn. (8)]. How-

$$2\ PhBr + 2e \xrightarrow{10\%\ NiCl_2(dppe)} Ph\text{–}Ph + 2Br^- \quad (E \leq -2\ v\ vs.\ SCE) \qquad (8)$$

ever the electrochemical approach demonstrates the existence of a threshold potential, a fact rather difficult to show when a metal is used as the reductant. Indeed when electrolysis is performed at potentials less negative than −2 V vs. SCE, no biphenyl is obtained, but two Faradays per mole of nickel complex are used and one equivalent of bromobenzene is consumed to yield eventually a phenylnickel(II) derivative, $Ph\text{–}Ni^{II}(dppe)Br$. Such a phenomenological observation acquires extreme importance when it is compared with the cyclic or steady-state voltammetry of $NiCl_2$(dppe) in the absence or in the presence of PhBr. As shown in Fig. 3, in the absence of PhBr, reduction of $NiCl_2$(dppe) occurs in two one-electron waves, R_1 and R_2 [eqns. (9) and (10)].

$$Ni^{II}Cl_2(dppe) + e \rightarrow Ni^{I}Cl(dppe) + Cl^- \quad (R_1,\ E_{1/2} = -0.80\ V) \qquad (9)$$

$$Ni^{I}Cl(dppe) + e \rightarrow Ni^{0}Cl(dppe) + Cl^- \quad (R_2,\ E_{1/2} = -1.35\ V) \qquad (10)$$

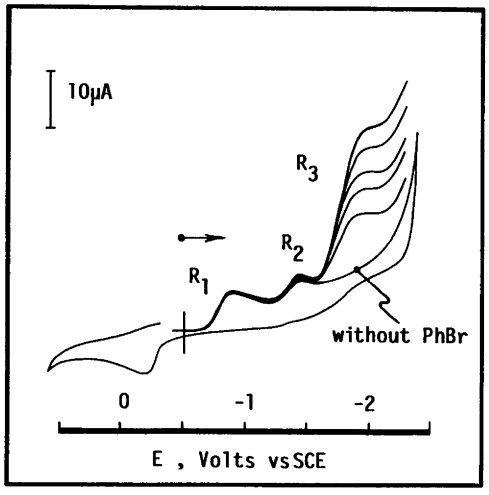

Fig. 3. Cyclic voltammetry of $Ni^{II}Cl_2$(dppe), 2 mM, in THF/HMPA (2/1 v/v), 0.1 M NBu_4BF_4 at 20 °C, in the absence or in the presence of different excesses of bromobenzene (from bottom to top: 0, 5, 7, 10, 21 and 31 equiv.). Stationary gold disc electrode, Ø 1.5 mm. Scan rate 0.2 V s^{-1}.

In the presence of bromobenzene, the development of a third wave is observed, R_3 ($E_{1/2} \approx -1.8V$), which can be shown independently to correspond to the one-electron reduction of a phenylnickel(II) complex formed by oxidative addition of PhBr to the zero-valent nickel electrogenerated at wave R_2 [eqns. (11) and (12)]. Moreover,

$$PhBr + Ni^0(dppe) \rightarrow Ph\text{–}Ni^{II}Br(dppe) \quad (11)$$

$$Ph\text{–}Ni^{II}Br(dppe) + e \rightarrow Ph\text{–}Ni^{I}(dppe) + Br^- \ (R_3) \quad (12)$$

from fast cyclic voltammetry the rate of the oxidative addition in eqn. (11) has been determined to be $10^5\ M^{-1}\ s^{-1}$, i.e. several orders of magnitude greater than those corresponding to chemically saturated zero-valent nickel complexes.[6a,15] This shows the considerable reactivity of poorly ligated zero-valent transition metals *vis-à-vis* their saturated analogs. Indeed these latter must undergo two successive de-ligandation steps before they can react in oxidative additions. For example in the case of a phosphine ligand, (denoted P) the two equilibria of eqns. (13) and (14) are involved prior to the oxidative addition step [eqn. (15)].

$$Ni^0P_4 \rightleftharpoons Ni^0P_3 + P \ (K_1) \quad (13)$$

$$Ni^0P_3 \rightleftharpoons Ni^0P_2 + P \ (K_2) \quad (14)$$

$$Ni^0P_2 + ArX \rightarrow Ar\text{–}Ni^{II}XP_2 \ (k) \quad (15)$$

For most common solvents and experimental conditions, K_1 is sufficiently large for the equilibrium in eqn. (13) to be displaced towards the right-hand side.[6] Conversely, although not known, K_2 is sufficiently small for eqn. (14) to act as a rapid pre-equilibrium, so that the experimental rate constant is $k^{app} = kK_2 << k$.[6] For example $Ni^0(dppe)_2$ undergoes no oxidative addition with PhBr, showing that in this case $K_2 \approx 0$, owing to the chelating properties of the dppe ligand. This corresponds to vanishingly small amounts of the catalyst in an active form, and therefore to a vanishingly small overall rate constant of oxidative addition. Instead, at an electrode or at a reducing metal particle surface, the zero-valent nickel $Ni^0(dppe)$, akin to Ni^0P_2 in eqn. (15), is generated quantitatively in the absence of excess ligand. Such effects alone may easily explain the considerably increased efficiency of reagents consisting of catalytic amounts of transition metal(II) salts together with a stoichiometric or excess quantity of reductant, with respect to the use of a stoichiometric transition metal under its zero-valent form.[3]

Let us now examine the fate of the electrogenerated phenylnickel(II) complex. In preparative electrolytic experiments, the observation of a threshold potential located just before the reduction wave of this intermediate demonstrates that its formation is not sufficient to allow reaction in eqn. (8) to proceed. Extra one-electron activation of $Ph\text{–}Ni^{II}Br(dppe)$ is required, since the electrolysis potential must be located on the plateau of the R_3 electrochemical wave [eqn. (12)]. Detailed examination of this wave shows that its current plateau value increases with the bromobenzene concentration [note that under our experimental conditions, bromobenzene is not reducible in the range of potential considered]. This behavior, reminiscent of redox catalysis[16] establishes that the phenylnickel(II) derivative is continuously regenerated at the electrode surface. Moreover, it is noticed from Fig. 4(b), that at low concentrations in bromobenzene, n_{R_3}, the number of electrons exchanged at wave R_3, is linearly dependent on the square root of the bromobenzene concentration and is independent of the nickel concentration. This demonstrates[16] that the phenylnickel(II) is regenerated through a kinetic sequence initiated by the reaction between its one-electron reduction product, $Ph\text{–}Ni^{I}(dppe)$, and bromobenzene [eqns. (16) and (17)].

$$Ph\text{–}Ni^{II}Br(dppe) + e \rightarrow Ph\text{–}Ni^{I}(dppe) + Br^- \quad (16)$$

$$Ph\text{–}Ni^{I}(dppe) + PhBr \rightarrow \cdots \rightarrow Ph\text{–}Ni^{II}Br(dppe) + \text{etc.} \quad (17)$$

At larger concentrations of bromobenzene n_{R_3} tends to level, and remains independent of the nickel concentration which evidences that the overall rate of the sequence described by eqn. (17) is now controlled by a step zero-order in bromobenzene and first order in nickel. The simplest reaction sequence compatible with these electrochemical data, which is in agreement with general chemical expectations[3,6–8] is as shown in eqns. (18)–(21).

$$Ph\text{–}Ni^{I}(dppe) + PhBr \rightarrow (Ph)_2Ni^{III}Br(dppe) \quad (18)$$

$$(Ph)_2Ni^{III}Br(dppe) \rightarrow Ph\text{–}Ph + Ni^{I}Br(dppe) \quad (19)$$

$$Ni^{I}Br(dppe) + e \rightarrow Ni^0(dppe) + Br^- \quad (20)$$

$$Ni^0(dppe) + PhBr \rightarrow Ph\text{–}Ni^{II}Br(dppe) \quad (21)$$

Indeed, as established above, reduction of $Ni^{I}Br(dppe)$ is largely exergonic* for electrode potentials located at the level of wave R_3; similarly within the timescale of steady-state voltammetry, the oxidative addition step in eqn. (21) is sufficiently fast not to be involved in the kinetic control of the overall sequence in eqns. (18)–(21). The rate of this sequence is then controlled by the slower step between eqns. (18) and (19). Thus at low PhBr concentrations oxidative addition of bromobenzene to the phenylnickel(I) derivative forces the overall rate to be first order in nickel and first order in PhBr, as observed experimentally. Conversely, at larger bromobenzene concentrations this step becomes sufficiently fast for the rate-determining step to be the reductive elimination of biphenyl from the nickel(III) species in eqn. (19). It is then seen that the sequence in

* Compare e.g. wave R_2, since the reduction potentials of $Ni^{I}X(dppe)$ do not depend critically on the nature of the halide X.[5]

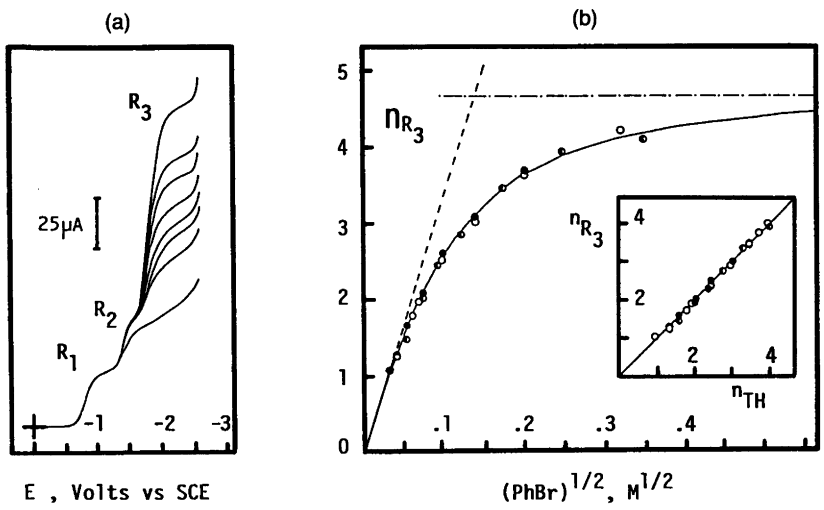

Fig. 4. Steady-state voltammetry of $Ni^{II}Cl_2$(dppe), 2 mM, in THF/HMPA (2/1 v/v), 0.1 M NBu_4BF_4 at 20 °C. (a) Steady-state voltammograms at a rotating gold disk electrode, ∅ 2 mm, in the absence or in the presence of different excesses of bromobenzene (from bottom to top: 0, 1, 2, 3, 5, 10, 20 and 50 equiv.). Scan rate 0.02 V s^{-1}; rotation rate 105 rad s^{-1}. (b) Experimental variations of $n_{R_3} = i^{lim}_{R_3}/i^{lim}_{R_1}$, as a function of bromobenzene concentration for [$Ni^{II}Cl_2$(dppe)] = 1 (●), 2 (○) and 3 (◐) mM. (——) Theoretical variations predicted for the mechanism in Scheme 1; (-----) limiting first-order dependence with bromobenzene concentration [rds eqn. (18)]; (·—·—·) limiting zero-order dependence with bromobenzene concentration [rds eqn. (19)]. The experimental (n_{R_3}) and theoretical (n_{TH}) values of n_{R_3} are also compared in the insert in (b).

eqns. (18)–(21) is in qualitative agreement with the above electrochemical observations.

In the following we present further advantages of the electrochemical approach in the investigation of such complex kinetic schemes. Since diffusion of molecules at an electrode surface is easily modelled, one can derive the theoretical rate law corresponding to a given sequence of reaction and compare its predictions with the actual experimental data. This is exemplified in Fig. 4(b), for the mechanism of biphenyl formation from bromobenzene in eqns. (16) and (18)–(21), in the form of the solid theoretical line which compares the predicted, n_{TH}, and experimental, n_{R_3}, values of the number of electrons exchanged at wave R_3. This allows quantitative assessment of the validity of the kinetic sequence presented in eqns. (16) and (18)–(21), and the determination of the rate constants of the two reactions which alternatively control the overall kinetics. Thus $k_1 = 10^3$ M^{-1} s^{-1} and $k_2 = 20$ M^{-1} s^{-1} were measured respectively for the oxidative addition in eqn. (18) and for the reductive elimination in eqn. (19).[5]

Nickel-catalyzed activation of bromobenzene in the presence of carbon dioxide.[17] In the preceding section we showed that electrochemical activation of bromobenzene in the presence of catalytic amounts of a nickel(II) salt is a convenient means of synthesizing biphenyls, with almost no formation of by-products. However, when the same experiment is performed in the presence of stoichiometric amounts of carbon dioxide, the formation of biphenyl is no longer observed but only that of benzoic acid[17,18] [eqn. (22)].

$$PhBr + CO_2 + 2e \rightarrow Ph\text{–}CO_2^- + Br^- \quad (E \leq -2 \text{ V vs. SCE}) \qquad (22)$$

This is a puzzling observation since the high efficiency of the biphenyl synthesis has been shown above to be a direct consequence of the fast sequence of reactions featured in Scheme 1, which develops without a significant termination step.† Thus one must conclude either that the biphenyl chain is no longer triggered in the presence of CO_2, or that one of its key intermediates is intercepted by CO_2. Let us examine successively each possibility in the following.

Fig. 5 shows that the transient or steady-state electrochemistry of $Ni^{II}Cl_2$(dppe) is independent of the presence of saturated CO_2 in the solution. This shows that none of the intermediates of eqns. (23)–(25) react with CO_2 within a time-scale where the carboxylation chain is fully operative.[19]

$$Ni^{II}Cl_2(dppe) + CO_2 \rightarrow \qquad (23)$$

$$Ni^{I}Cl(dppe) + CO_2 \rightarrow \qquad (24)$$

$$Ni^{0}(dppe) + CO_2 \rightarrow \qquad (25)$$

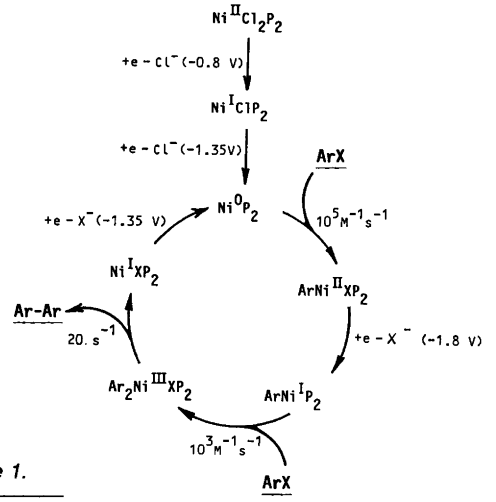

Scheme 1.

† The only termination step observed consists of deactivation of the nickel catalyst by a slow dimerization of the $Ni^{I}X$(dppe) species when the potential set is insufficiently cathodic ($E \geq -1.9$ V vs. SCE).

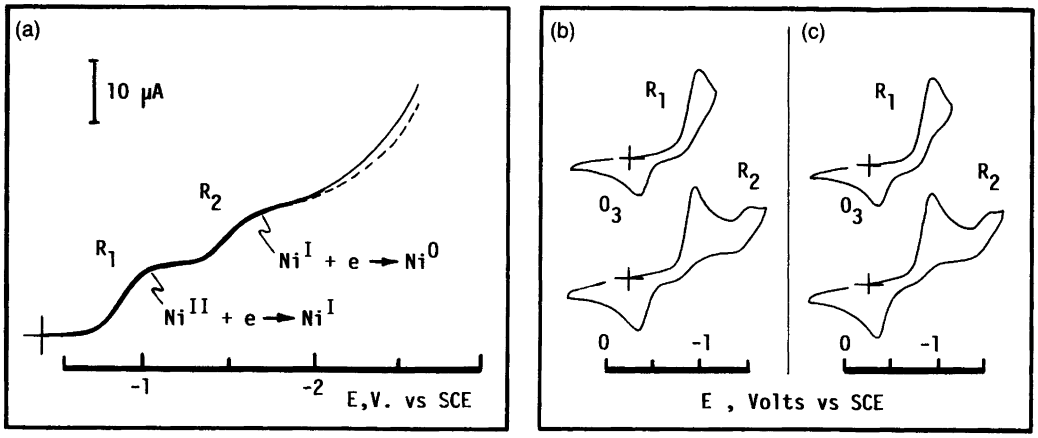

Fig. 5. Steady state (a) and cyclic voltammetry of $Ni^{II}Cl_2$(dppe), 2 mM, in THF/HMPA (2/1 v/v), 0.1 M NBu_4BF_4 at 25 °C, in the absence or in the presence of saturated (≈ 0.08 M) carbon dioxide. (a) Steady state voltammetry (scan rate 0.020 V s^{-1}) at a gold disk rotating electrode, ∅ 2 mm, with (——) or without (-----) CO_2. (b,c) Cyclic voltammetry at a stationary gold disk electrode, ∅ 0.5 mm, without (b) or with (c) CO_2. Scan rate 0.10 V s^{-1}; inversion potential: −1.1 (top voltammograms) and −1.65 (bottom voltammograms) V vs. SCE.

We must therefore conclude that in the presence of CO_2, the poorly ligated zero-valent nickel Ni^0(dppe) still reacts with PhBr via fast oxidative addition in eqn. (21) (see also below), which results in the initiation of the chain reaction in Scheme 1. Since Ni^IX(dppe) is also unreactive with CO_2 [eqn. (24)], the biphenyl chain must be interrupted by the reaction of CO_2 with one of the three remaining intermediates involved in the chain propagation: Ph–Ni^{II}Br(dppe), Ph–Ni^I(dppe) or $(Ph)_2Ni^{III}$(dppe). Ph–Ni^{II}Br(dppe) can be excluded since Fig. 6(a) shows that its reduction wave, R_3, is still present, and that it even increases in the presence of CO_2. Moreover, the success of the reaction in eqn.(22) requires the electrolysis to be performed on the plateau of wave R_3, i.e. at $E \leq -2$ V vs. SCE, which establishes that Ph–Ni^I(dppe) must be produced for the carboxylation step to proceed. $(Ph)_2Ni^{III}$(dppe) involvement can also be easily rejected. Indeed if this last were an intermediate in the carboxylation chain, the maximum rate of carboxylation could not exceed that of PhBr oxidative addition to Ph–Ni^I(dppe). In other words, for a given concentration in PhBr, all values of n_{R_3} obtained in the presence of CO_2 should be located under the dashed line represented in Fig. 6(b), which corresponds to the initial slope in Fig. 4(b). This clearly contradicts the experimental observations reported in Fig. 6(b), which rules out any possible participation of $(Ph)_2Ni^{III}$(dppe) in the carboxylation chain.

At this point we have established that the branching of the biphenyl and carboxylation chains occurs at the level of the Ph–Ni^I(dppe) intermediate. We also know from the data in Fig. 6(b), that this species reacts considerably faster with CO_2 than with PhBr, which explains why the biphenyl step decreases in the presence of stoichiometric amounts of carbon dioxide. Yet it is not clear whether Ph–Ni^I(dppe) reacts in one step with CO_2, e.g. via CO_2 insertion into the

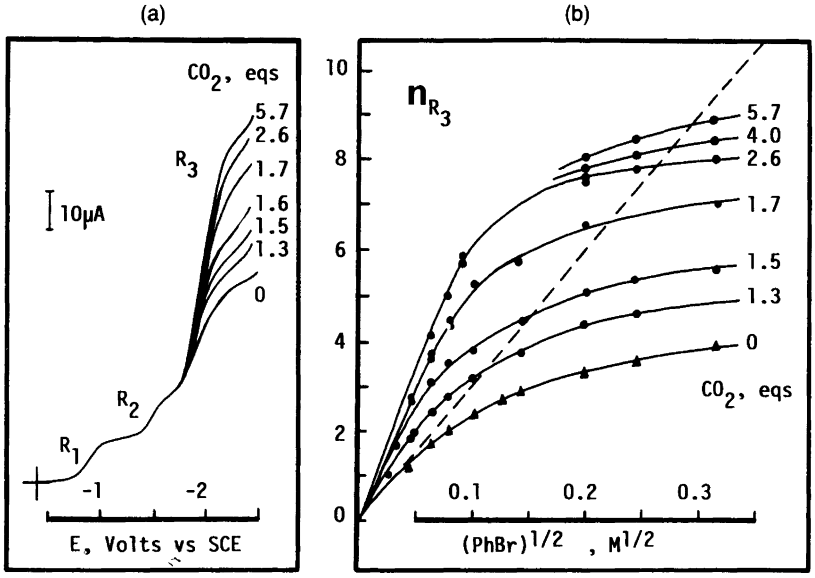

Fig. 6. Steady-state voltammetry of $Ni^{II}Cl_2$(dppe), 2 mM, in THF/HMPA (2/1 v/v), 0.1 M NBu_4BF_4 at 25 °C (scan rate 0.020 V s^{-1}) at a gold disk rotating electrode, ∅ 2 mm. (a) Steady-state voltammograms in the presence of 10 equivs. of bromobenzene and in the absence or in the presence of various equivalents (numbers on the curves) of carbon dioxide. (b) Variations of the number of electrons, n_{R_3}, exchanged at wave R_3 as a function of the bromobenzene and carbon dioxide concentrations.

phenyl–nickel bond,[19a] to yield a nickel(I) carboxylate derivative [eqn. (26)], or whether reaction (26) consists of a

$$Ph\text{–}Ni^{I}(dppe) + CO_2 \rightarrow PhCO_2\text{–}Ni^{I}(dppe) \quad (26)$$

sequence of two or more elemental steps. If eqn. (26) is a truly elemental step the carboxylation chain would be as in Scheme 2. From this scheme it is seen that, since all electron transfers are exergonic under our electrochemical conditions, the only possible rate-determining steps for the chain are either oxidative addition of PhBr to Ni^0(dppe) or reaction between Ph–Ni^I(dppe) and CO_2. Therefore the chain-propagation rate, and therefore n_{R_3} values, should increase when PhBr and/or CO_2 concentrations are increased. This prediction disagrees with the experimental facts in Fig. 7(a), since n_{R_3} tends to level when [CO_2] or [PhBr] are increased, as shown respectively by the data in Figs. 7(a) and 6(b).

As already discussed a saturation effect such as that represented in Fig. 7(a) proves that the propagation rate of the carboxylation is kinetically controlled by a step first order in nickel species but zero order in CO_2 or PhBr. Therefore eqn. (26) must consist of at least two steps, the former being between CO_2 and Ph–Ni^I(dppe), which affords a new nickel species, the latter yielding the nickel(I) carboxylate. By analogy with eqns. (18) and (19) we propose that the first step corresponds to an oxidative addition of CO_2 to the phenylnickel(I) derivative, in a way similar to the reaction of CO_2 with some zero-valent nickel complexes.[19] This would afford a nickel(III) species which would undergo reductive elimination of the benzoate moiety, the latter remaining co-ordinated to the resulting nickel(I) intermediate and being released upon reduction, eqn. (29).

$$Ph\text{–}Ni^{I}(dppe) + CO_2 \rightarrow Ph\text{–}Ni^{III}(CO_2)(dppe) \quad (27)$$

$$Ph\text{–}Ni^{III}(CO_2)(dppe) \rightarrow PhCO_2\text{–}Ni^{I}(dppe) \quad (28)$$

$$Ph\text{–}CO_2\text{–}Ni^{I}(dppe) + e \rightarrow Ni^{0}(dppe) + PhCO_2^{-} \quad (29)$$

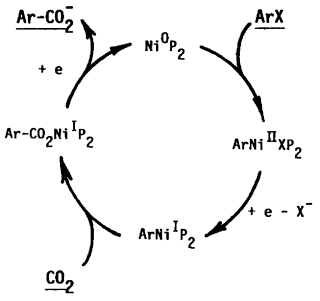

Scheme 2.

Incorporating these reactions into those already established implies the chain mechanism in Scheme 3 for the nickel-catalyzed carboxylation of aryl halides with a reductive driving force. As for the biphenyl chain mechanism in Scheme 1, it is noteworthy that this cycle involves different nickel complexes, some diamagnetic and others paramagnetic. We have shown above how semiquantitative deductions based on electrochemical data can be used to identify the different steps involved in a complex mechanistic sequence. To conclude this section we show that quantitative exploitation of the same data can be used to confirm further and to quantify these results.

Under our electrochemical conditions, three possible steps may compete for the kinetic control of the propagation of the chain sequence represented in Scheme 3: (i) oxidative addition of PhBr to Ni^0(dppe), with a rate constant k_{PhBr} in eqn. (21); (ii) oxidative addition of CO_2 to Ph–Ni^I(dppe), with a rate constant k_{CO_2} in eqn. (27); or (iii) the reductive elimination of benzoate, with a rate constant k_{elim} in eqn. (28). Indeed as already noted with regard the biphenyl chain all the electrochemical steps are sufficiently exergonic when the cathode potential is set more negative than −2 V vs. SCE, not to be directly involved in the kinetic control of the chain propagation. On the other hand, we know from the data in Figs. 6(b) and 7(a) that n_{R_3} values tend to level when PhBr or CO_2 concentrations are increased, which is direct evidence that these parameters exert only slight kinetic influence, i.e. that the reductive elimination of benzoate is the main factor controlling the propagation rate. Under these conditions one can show

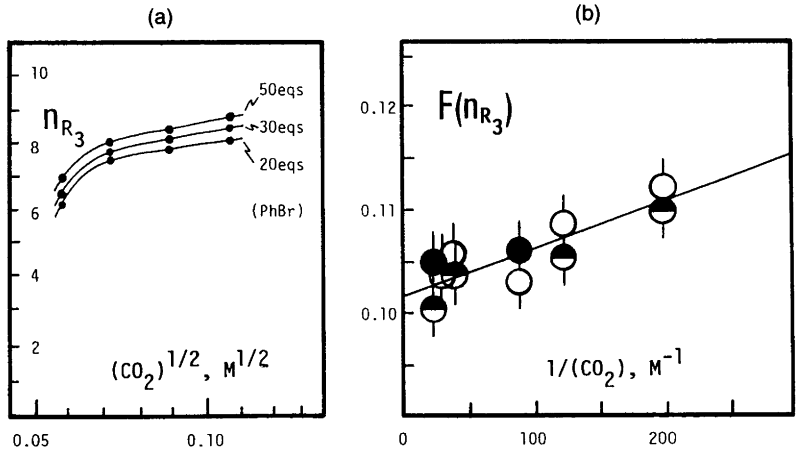

Fig. 7. Steady-state voltammetry of $Ni^{II}Cl_2$(dppe), 2 mM, in THF/HMPA (2/1 v/v), 0.1 M NBu_4BF_4 at 25 °C (scan rate 0.020 V s^{-1}) at a gold disk rotating electrode, ∅ 2 mm. (a) Variations of the number of electrons, n_{R_3}, exchanged at wave R_3 [compare Fig. 6(a)] as a function of the bromobenzene and carbon dioxide concentrations. (b) Variations of $F(n_{R_3}) = \{[(2\delta/D^{1/2})/(1+n_{R_3})] - (k_{PhBr}[PhBr])^{-1/2}\}$, as a function of (1/[$CO_2$]). See the text for the definition of the various parameters used in the formulation of $F(n_{R_3})$. PhBr: 20 (●), 30 (○) and 50 (◓) equivs. per nickel complex.

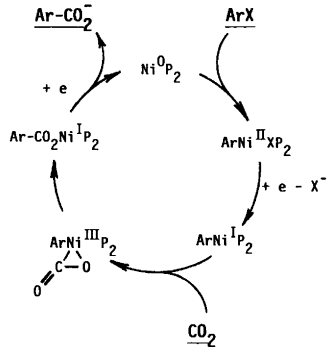

Scheme 3.

that n_{R_3} must obey the eqn. (30),[20] where δ (ca. 9×10^{-4} cm)[5] is the diffusion layer thickness and D (ca. 3×10^{-6}

$$(2\delta/D^{1/2})/(1+n_{R_3}) = (k_{elim})^{-1/2} + \{(k_{elim})^{1/2}/(k_{cos}[CO_2])\} + (k_{PhBr}[PhBr])^{-1/2} \quad (30)$$

$cm^2\ s^{-1}$)[5] is the average diffusion coefficient of the nickel species. However, the last term on the right-hand side of eqn. (30) can be evaluated independently since $k_{PhBr} = 10^5$ $M^{-1}\ s^{-1}$, was determined above in the study of the biphenyl chain.[5] Eqn. (30) then predicts that $F(n_{R_3}) = \{[(2\delta/D^{1/2})/(1+n_{R_3})]-(k_{PhBr}[PhBr])^{-1/2}\}$ should vary linearly with $(1/[CO_2])$, with a slope $p = \{(k_{elim})^{1/2}/(k_{CO_2}[CO_2])\}$. From the intercept, $(k_{elim})^{-1/2}$, of such a plot presented in Fig. 7(b), one can determine the rate constant of the benzoate reductive elimination in eqn. (28), i.e. $k_{elim} \approx 10^2\ s^{-1}$. The linear dependence with $(1/[CO_2])$ predicted by eqn. (30) is more difficult to ascertain since the observed variations are comparable to the experimental uncertainties. Nevertheless, from the regression line drawn on Fig. 7(b), one can deduce that the rate constant, k_{CO_2}, of the oxidative addition of CO_2 to Ph–Ni^I(dppe) in eqn. (27), is of the order of ca. $1\text{–}2\times10^5\ M^{-1}\ s^{-1}$.

The magnitude of k_{CO_2} explains why the biphenyl chain is totally annihilated when carbon dioxide is present in the reaction medium. Indeed, since the rate constant of CO_2 oxidative addition to the phenylnickel(I) intermediate is ca. 100 to 200 times larger than that of bromobenzene, it is understood that as soon as CO_2 is present in stoichiometric amounts, i.e. when its concentration is of the order of that of bromobenzene, more than 99% of the Ph–Ni^I(dppe) molecules are forced into the carboxylation route. Yet this does not mean that the carboxylation chain is intrinsically faster than the biphenyl one. Indeed, the carboxylation chain propagation rate cannot exceed that of the reductive elimination in eqn. (28). Similarly, in the absence of CO_2 the biphenyl chain cannot propagate faster than the rate of biphenyl reductive elimination in eqn. (19). Since the rate constants of these two steps are $100\ s^{-1}$ and $20\ s^{-1}$, respectively, it is easily understood that the maximum propagation rates of the two chains are comparable, in agreement with the experimental observation of close n_{R_3} maximum values for both chains [cf. e.g. Figs. 4 and 7(a)].

Conclusions

We have tried to prove in this paper that electrochemical data can be used to great advantage in the investigation of complex reaction schemes. Mechanistic conclusions can be easily drawn from qualitative or semiquantitative electrochemical observations. More quantitative analyses are also possible, and serve further to confirm mechanistical interpretations and eventually to determine the corresponding rate constants. However one may still wonder if the data and mechanisms arising from such electrochemical approaches, have any relevance to more usual 'homogeneous' chemistry, i.e. to non-electrochemical conditions.

In the introduction of this paper, we gave a positive answer to this question, based on the striking conceptual analogies that exist between electrochemistry and 'homogeneous' chemistry. As a conclusion to this work we would like to show that this is not only a matter of subtle concepts, but also that it happens to be true in the experimental practice.

Let us consider for example the nickel-catalyzed formation of biphenyl from aryl halides at zinc particles. From Scheme 1, which summarizes most of the kinetic data obtained electrochemically, it is easily seen that when zinc is used as a reductant instead of an electrode, the slowest step of the chain is the difficult reduction of the arylnickel(II) intermediate. In such a case the rate of the reaction is independent of the aryl halide concentration but is first order in zinc and first order tin Ar–Ni^{II}Br(dppe). However, most of the nickel catalyst is 'stored' under the form of the latter since its consumption is the rate-determining step of the chain. Therefore the arylnickel(II) concentration is close to that of the initial nickel complex, denoted hereafter as [Ni]. From these simple considerations it is predicted that the rate of disappearance of the aryl halide is given by eqn. (31), where k_{Zn} is an apparent rate constant depending on the local hydrodynamics and on the size and surface state of the zinc particles (see above).

$$d[ArX]dt = -2d[ArAr]/dt = -k_{Zn}[Zn][Ni] \quad (31)$$

Eqn. (31) should remain valid except at the end of the reaction, i.e. when the aryl halide concentration tends to zero. Then the slowest step of the chain becomes the oxidative addition of the aryl halide to the arylnickel(I) species, and the overall rate of the reaction is given by eqn. (32) where k^* depends on the true rate constant of the oxidative addition, as well as on the solution hydrodynamics. One may find it puzzling that eqn. (32) depends on the

$$d[ArX]/dt = -2d[ArAr]/dt = -k^*[Zn][ArX][Ni] \quad (32)$$

'zinc concentration,' although the rate-determining step is formally first order in aryl halide, first order in arylnickel(I) and zero-order in zinc. Yet it must be recalled that all the chemical steps considered in Scheme 1 occur within the diffusion layer existing around each zinc particle, while the

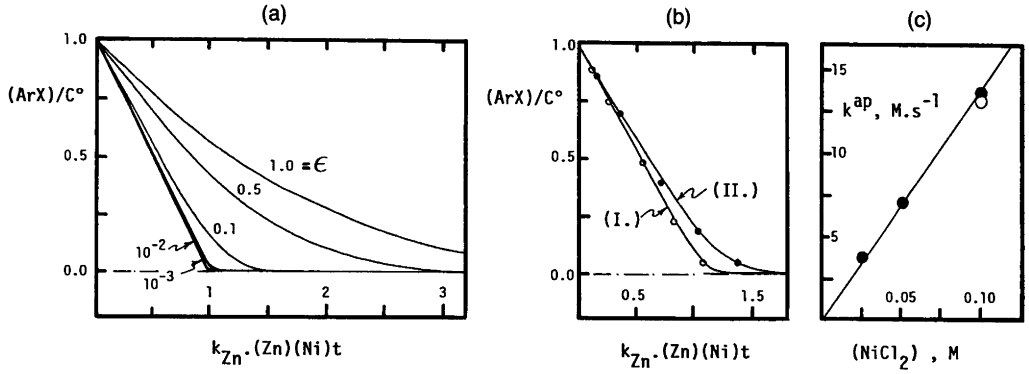

Fig. 8. 'Homogeneous' biphenyl formation from chlorobenzene by nickel–TPP complexes in the presence of zinc powder. (a) Theoretical variations of chlorobenzene concentration (initial concentration C^0) as a function of time for different values of $\varepsilon = k_{Zn}/(k^*C^0)$, according to eqn. (34). [Ni] concentration of nickel complex; [Zn] equivalent concentration of zinc. See the text for the definition of k_{Zn} and k^*. (b) Comparison between the theoretical predictions in (a) and the experimental data reported by Colon and Kelsey.[3] (I) Experimental: $NiCl_2$ (1 mmol), TPP (7.6 mmol), Zn (30.6 mmol), NaBr (9.7 mmol) and PhCl (19.7 mmol); Theoretical: k_{Zn}[Zn][Ni] = 0.55 min^{-1} and $\varepsilon = 0.05$. (II) Experimental: $NiCl_2$ (1 mmol), TPP (3.81 mmol), Zn (30.6 mmol), NaBr (4.86 mmol) and PhCl (9.8 mmol); Theoretical: k_{Zn}[Zn][Ni] = 0.068 min^{-1} and $\varepsilon = 0.13$. (c) Variations of k^{ap}, the apparent rate constant for biphenyl formation deduced from initial slopes, as a function of the nickel complex concentration. Experimental data from Table 5 in Ref. 3: [NaBr] = 1 M, [PhCl] = (○) 1 or (●) 2 M.

overall rate in eqn. (32) is defined with respect to the volume of the bulk solution. This implies that the overall rate of formation of biphenyl is proportional to the zinc surface area per volume of solution, that is to the 'zinc concentration,' for even particles.

In a more general case, i.e. when both steps compete for kinetic control of the chain propagation, eqns. (31) and (32) have to be replaced by the general eqn. (33) which tends to the limiting forms in eqn. (31) or (32) depending on the magnitude of the term $\{k_{Zn}/(k^*[ArX])\}$.

$$d[ArX]/dt = -2d[ArAr]/dt = -k_{Zn}[Zn][Ni]/\{1 + k_{Zn}/(k^*[ArX])\} \quad (33)$$

$$1 - [ArX]/C^\circ - \varepsilon\ln([ArX]/C^\circ) = k_{Zn}[Zn][Ni]t \quad (34)$$

When an excess of zinc is used, integration of eqn. (33) affords eqn. (34), where C° is the initial concentration of the aryl halide, and $\varepsilon = k_{Zn}/(k^*C^\circ)$). In Fig. 8(a) are presented the variations of ([ArX]/C°) as a function of time for different values of ε, according to the rate law in eqn. (34). It is seen from Fig. 8(b) that these predictions, based on Scheme 1, i.e. on electrochemical data, are in remarkable agreement with the experimental variations observed by Colon and Kelsey,[3] for the 'homogeneous' nickel ($NiCl_2$/triphenylphosphine)-catalyzed coupling of chlorobenzene in the presence of an excess of zinc. Besides demonstrating that transposition of electrochemical data to non-electrochemical conditions is possible, Fig. 8(b) allows quantitative mechanistic conclusions to be drawn. For example, the initial slopes of the data in Fig. 8(b) are mainly related to the magnitude of the term $\{k_{Zn}$[Zn][Ni]} in eqn. (34) [compare, e.g., Fig. 8(c)], whereas the curvature of the plots, i.e. the departure from a zero-order dependence in chlorobenzene, is related to the magnitude of $\varepsilon = k_{Zn}/(k^*C^\circ)$. Therefore, use of this model allows the quantitative investigation of the effect of experimental conditions on each rate constant k_{Zn} and k^*.

Acknowledgements. This work was supported by CNRS (UA 1110 *Activation Moléculaire*) and *Ecole Normale Supérieure.* Additional support from *Electricité de France* and *Société Nationale des Poudres et Explosifs* is also gratefully acknowledged.

References

1. (a) Semmelhack, M. F., Helquist, P. M. and Jones, L. D. *J. Am. Chem. Soc. 93* (1971) 5908; (b) Semmelhack, M. F. and Ryono, L. S. *J. Am. Chem. Soc. 97* (1975) 3873; (c) Semmelhack, M. F., Helquist, P. M., Jones, L. D., Keller, L., Mendelson, L., Ryono, L. S., Smith, J. G. and Stauffer, R. D. *J. Am. Chem. Soc. 103* (1981) 6460.
2. Zembayashi, M., Tamao, K., Yoshida, J. and Kumada, M. *Tetrahedron Lett.* (1977) 4089.
3. Colon, I. and Kelsey, D. R. *J. Org. Chem. 51* (1986) 2627.
4. See e.g., Troupel, M., Rollin, Y., Perichon, J. and Fauvarque, J. F. *Nouv. J. Chim. 5* (1981) 621.
5. Amatore, C. and Jutand, A. *Organometallics 7* (1988) 2203.
6. (a) Tsou, T. T. and Kochi, J. K. *J. Am. Chem. Soc. 101* (1979) 6319; (b) *J. Am. Chem. Soc. 101* (1979) 7547; (c) *J. Org. Chem. 45* (1980) 1930.
7. See Refs. 3, 6 and references and discussions therein. See also: (a) Parshall, G. W. *J. Am. Chem. Soc. 96* (1974) 2360; (b) Hidai, M., Kashiwagi, T., Ikenchi, T. and Uchida, Y. *J. Organomet. Chem. 30* (1971) 279; (c) Fahey, D. R. *J. Am. Chem. Soc. 92* (1970) 402; (d) Fahey, D. R. *Organomet. Chem., Rev. Ser. A 7* (1972) 245; (e) Fahey, D. R. and Mahan, J. E. *J. Am. Chem. Soc. 99* (1977) 2501.
8. (a) Almemark, M. and Åkermark, B. *J. Chem. Soc., Chem. Commun.* (1978) 66; (b) Morell, D. G. and Kochi, J. K. *J. Am. Chem. Soc. 97* (1975) 7262. For stable diarylnickel(III) complexes see: (c) Grove, D. M. van Koten, G. and Zoet, R. *J. Am. Chem. Soc. 105* (1983) 1379; (d) Grove, D. M., van

Koten, G., Mul, W. P., van der Zeijde, A. A. H., Zoutberg, M. C. and Stam, C. H. *Organometallics 5* (1986) 322.
9. Ref. 3, p. 2635.
10. See e.g. Levich, V. G. *Physicochemical Hydrodynamics,* Prentice-Hall, Englewood Cliffs, NJ 1962.
11. See e.g. (a) Baranov, S. N., Dumbai, M. A. and Krivun, S. W. *Khim. Het. Soed.* (1972) 1313; (b) Fabre, C., Fugnitto, R. and Strzelecka, H. *C. R. Acad. Sci. Paris 282* (1976) 175; (c) Gionis, V., Fugnitto, R., Meyer, G., Strzelecka, H. and Dubois, J. C. *Mol. Cryst. Liq. Cryst. 90* (1982) 153.
12. Amatore, C. A., Jutand, A. and Pflüger, F. *J. Electroanal. Chem. 218* (1987) 361.
13. See e.g. Amatore, C. In: Lund, H. and Baizer, M., Eds., *Organic Electrochemistry,* Marcel Dekker, New York 1990, Chap. 4.
14. A detailed analysis of this system is presented in Ref. 5.
15. Troupel, M., Rollin, Y., Sibille, S., Fauvarque, J. F. and Perichon, J. *J. Chem. Res. (S)* (1980) 24.
16. Andrieux, C. P. and Savéant, J. M. In: Bernasconi, C. F., Ed., *Investigation of Rates and Mechanisms of Reactions,* Wiley, New York 1986, Vol. 6, 4/E. Part 2, Chap. 7, pp. 305–390.
17. The complete and detailed analysis of this reaction will be presented elsewhere: Amatore, C. and Jutand, A. *Unpublished work.*
18. Fauvarque, J. F., Chevrot, C., Jutand, A., François, M. and Perichon, J. *J. Organomet. Chem. 264* (1984) 273.
19. For reactions of CO_2 with other zero-valent nickel complexes cf. e.g. (a) Behr, A. *Angew. Chem., Int. Ed. Engl. 27* (1988) 661; (b) Behr, A. Keim, W. and Thelen, G. *J. Organomet. Chem. 249* (1983) C38; (c) Aresta, M. and Nobile, F. *J. Chem. Soc., Dalton Trans.* (1977) 708; (d) Döhring, A., Jolly, P. W., Krüger, C. and Romào, M. J. *Z. Naturforsch. 40* (1985) 484.
20. Amatore, C., Jutand, A. and Mottier, L. *Unpublished work.*

Received January 22, 1990.